Available online at www.sciencedirect.com
ScienceDirect
Journal of the European Ceramic Society 31 (2011) 2099–2106
www.elsevier.com/locate/jeurceramsoc

Influence of ionic mobility on the phase transformation route in $Y_3Al_5O_{12}$ (YAG) stoichiometry

Meng-Jung Li, Yu-Chun Wu *, Fu-Su Yen, Chi-Yuan Huang

Department of Resources Engineering, National Cheng Kung University, No. 1 University Road, Tainan 70101, Taiwan

Received 1 November 2010; received in revised form 11 April 2011; accepted 30 April 2011
Available online 31 May 2011

Abstract

Ionic mobilities of Y^{3+} and Al^{3+} are controlled using either amorphous or well-crystallized precursors and enhanced by the addition of molten NaCl flux. Experimental results indicate that phase transformation prefers a relatively slow reaction route via YAM–YAP–YAG because of limited ionic mobility when either Y^{3+} or Al^{3+} is confined to a crystallized structure. The selection of intermediate phases can be either Y-rich (YAM) or Al-rich (YAP), depending on the competition of ionic mobility between Y^{3+} and Al^{3+} during phase transformation. The YAH–YAG route is selected only when the ionic mobility of Y^{3+} or Al^{3+} is high enough to induce a nucleation and growth reaction while a certain degree of stoichiometric inhomogeneity is presented; otherwise YAG is crystallized directly from amorphous precursors without passing through any intermediate phase.

Keywords: Hexagonal-YAP; Y_2O_3; Al_2O_3; Diffusion: Microstructural-final

1. Introduction

Yttrium aluminum garnet ($Y_3Al_5O_{12}$, YAG) is a widely used material due to its excellent optical and mechanical properties. It is generally believed that phase transformation in Y_2O_3–Al_2O_3 systems is comprised of a complex series of consecutive and parallel reactions that generate various intermediate products, such as $Y_4Al_2O_9$ (YAM), $YAlO_3$ perovskite (YAP), and hexagonal-YAP (YAH), before yielding a final stable YAG phase.[1–5] Neiman et al.[1] and Glushkova et al.[2] suggested that the formation of YAG is carried out by the diffusion of Al ions into the Y_2O_3 structure. This provides a fair explanation for the observation that $Y_4Al_2O_9$ (YAM) is often the first phase that appears at relatively lower temperatures during the Y_2O_3–Al_2O_3 solid-state reaction, and a temperature above 1500 °C is required to obtain the pure YAG phase.[6] Some researchers have indicated that the phase evolution in Y_2O_3–Al_2O_3 systems is affected by the presence of impurities. For example, carbon compounds induce oxygen vacancies that accelerate the phase transformation rate, whereas nitrate radicals suppress the transformation process.[7] Phase transformation via the YAH–YAG route is another typical phase selection route that is only observed during wet-chemical syntheses, such as sol–gel or precipitation processes.[3,8–11] In these synthetic methods, YAG can sometimes be crystallized directly from amorphous precursors at temperatures as low as 800–900 °C.[12–21] YAH is an extremely unstable phase that often transforms to YAG within a very short span of time. Hence, investigations that focus on observations of YAH and its formation mechanism are rare. Ullal et al.[13] suggested that the driving forces for the nucleation of the YAH or YAG phases are comparable, and one phase may be preferred when another phase is minimized. Other researchers have proposed that impurities are the key factors that dominate the phase selection route. For example, nitrate compounds easily induce YAH formation and carbon compounds more readily drive YAG crystallization directly from the amorphous phase.[7] Gandhi and Levi[22] claimed that the phase selection of YAG or YAH is not related to the homogeneity of the precursor but is biased by a difference in the structure of the amorphous phase; however the link between these differences and phase selection remains unclear. Generally, the phase transformation process for the synthesis of YAG seems related to the precursor types, where the solid-state reaction often follows the YAM–YAP–YAG route and YAH–YAG is more likely to occur in soft-chemical processes. The different phase transformation routes seem to be correlated with the ionic mobility of the precursors used. In the present work, attention is paid to the

* Corresponding author. Tel.: +886 6 2757575x62824; fax: +886 6 2380421.
E-mail address: yuchunwu@mail.ncku.edu.tw (Y.-C. Wu).

0955-2219/$ – see front matter © 2011 Elsevier Ltd. All rights reserved.
doi:10.1016/j.jeurceramsoc.2011.04.038

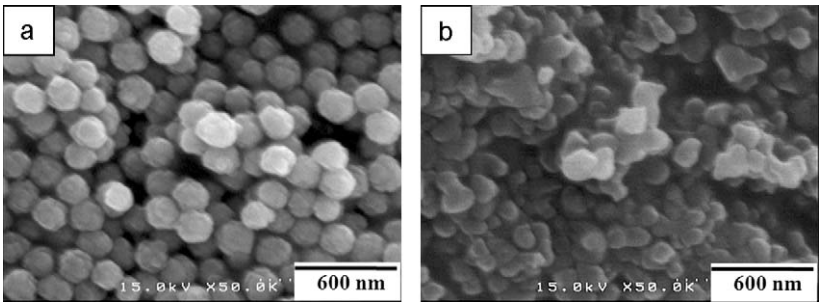

Fig. 1. SEM micrographs of crystallized precursors: (a) Y_2O_3 and (b) Al_2O_3 particles.

influence of ionic mobility on the phase transformation behaviors of YAG stoichiometry. Ionic mobility is modified using either amorphous or well-crystallized precursors and enhanced by the addition of molten NaCl flux. Experimental parameters are elaborated with the aim of inducing different phase transformation routes in YAG stoichiometry. A kinetic study on the phase transformation process under isothermal conditions is carried out in order to establish the correlation between the phase transformation route and the ionic mobility of the precursors.

2. Experimental

Monodispersed Y_2O_3 spheres (D_{50}: 200 nm) were synthesized by a urea-based homogeneous precipitation technique[23] and calcined at 1000 °C for 1 h to yield well-crystallized Y_2O_3 precursors. α-Al_2O_3 particles were purchased (Taimei Chemicals Co., Japan) and employed as precursors after a ball-milling treatment in water for 10 h. The average particle sizes of both Y_2O_3 and α-Al_2O_3 precursors were controlled to about 200 nm, as illustrated in Fig. 1, to eliminate size effects during phase transformation. Y_2O_3 spheres were added to an aluminum isopropoxide (AIP, 98+%, Aldrich, Germany)/isopropanol solution in YAG stoichiometry, i.e., $[Y^{3+}]/[Al^{3+}] = 0.6$. The suspension rapidly became milky white due to the hydrolysis reaction of AIP. The hydrated AIP colloidal particles were identified as amorphous structure according to their XRD patterns. An NH_4OH aqueous solution was added to adjust the pH value to 11 and keep the Y_2O_3 and the hydrated AIP colloidal particles oppositely charged, thus inhibiting inhomogeneous segregation. α-Al_2O_3 powders and [$Y(NO_3)_3{\cdot}6H_2O$] were mixed in deionized water, also in YAG stoichiometry, to obtain an homogeneous suspension. Both suspensions were stirred under room temperature for 180 min and then dried at 100 °C for 12 h to acquire the Y_2O_3 embedded in amorphous Al_2O_3 and the Al_2O_3 embedded in amorphous Y_2O_3 precursors, respectively. The as-dried precursors were ground in an alumina mortar to further increase mixing homogeneity. An analogue of the synthesis was performed to prepare the amorphous [Y_2O_3/Al_2O_3] precursor by drying a mixture of $Y(NO_3)_3{\cdot}6H_2O$ and AIP in isopropanol. The sample labels and their corresponding precursor types are listed in Table 1 where Al^{3+} and Y^{3+} in brackets denote the amorphous Al_2O_3 and amorphous Y_2O_3, respectively. For the second part of the experiment, dehydrated NaCl equivalent to 10 times the weight of the precursor powder was used as a flux for the samples described above. The precursors without NaCl were directly put into the tube furnace at 1600 °C in order to prevent the crystallization of the amorphous precursors during the heating process and held for various durations from 1 to 60 min. The heat treatments for the samples with NaCl were performed in a tube furnace at 1150 °C from 1 to 10 min while the crucible is sealed to prevent the evaporation of NaCl. The samples were immediately removed from the tube furnace and quenched to room temperature when the required heat treatments were completed. The samples annealed with NaCl were washed with deionized water after the heat treatments to remove the unreacted flux. The phase compositions as a function of the heat treatments were characterized by powder X-ray diffraction (Rigaku, Miniflex). Raman spectra were also recorded by Raman microscope (Renishaw inVia) with a He-Ne laser at 633 nm as an excitation source. Particle morphology observations were carried out by scanning electron (SEM, Hitachi 4100) and transmission electron microscopy (TEM, JEOL JEM 2100).

Table 1
Sample labels and their corresponding precursor types.

Sample label	Yttrium source	Aluminum source
[Y_2O_3/Al^{3+}]	Y_2O_3 sphere (200 nm)	Aluminum isopropoxide
[Al_2O_3/Y^{3+}]	($Y(NO_3)_3{\cdot}6H_2O$)	α-Al_2O_3 (200 nm)
[Y^{3+}/Al^{3+}]	($Y(NO_3)_3{\cdot}6H_2O$)	Aluminum isopropoxide

3. Results and discussion

3.1. YAM–YAP–YAG phase transformation route

Fig. 2 illustrates the XRD patterns of the [Y_2O_3/Al^{3+}] sample after heating at 1600 °C for 1, 5, 10, 30, and 60 min. The reaction between Y_2O_3 and amorphous Al_2O_3 occurs after 1 min at 1600 °C according to the appearances of YAM and YAP. A slight amount of α-Al_2O_3 is unavoidably crystallized from the amorphous Al_2O_3 since the heating temperature is quite high. YAG begins to emerge after 5 min and becomes the major phase after 10 min. The amount of unreacted Y_2O_3, α-Al_2O_3, YAM, and YAP decreases with increasing YAG. A pure YAG phase is eventually obtained when the holding time is 60 min. The phase evolution of this sample is similar to that observed in the conventional solid-state reaction of Y_2O_3 and Al_2O_3, in which

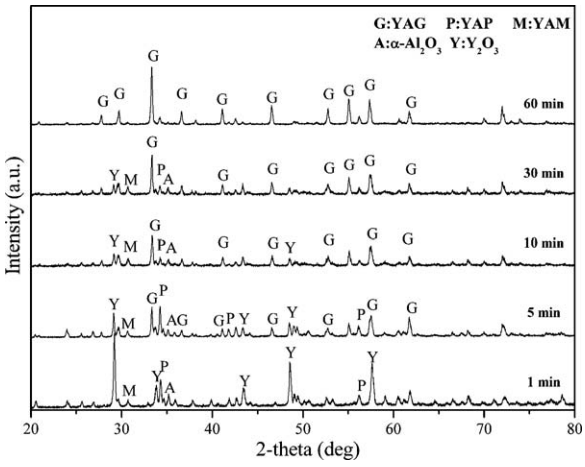

Fig. 2. XRD patterns of [Y_2O_3/Al^{3+}] annealed at 1600 °C for 1, 5, 10, 30, and 60 min.

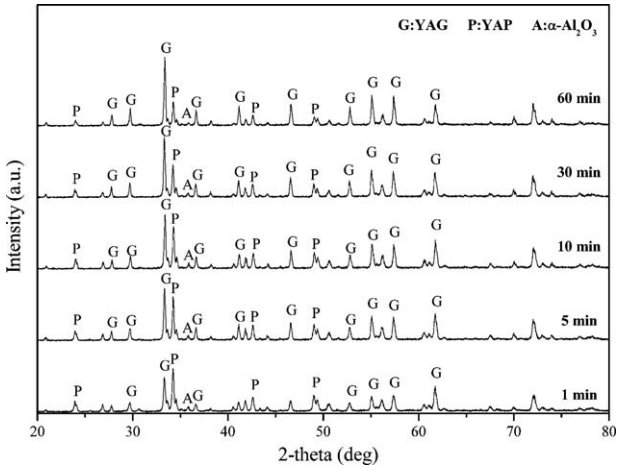

Fig. 4. XRD patterns of [Al_2O_3/Y^{3+}] annealed at 1600 °C for 1, 5, 10, 30, and 60 min.

the transformation sequences proceed by a series of reactions as below.[1–3]

$$Y_2O_3 + Al_2O_3 \rightarrow \text{YAM}$$

$$\text{YAM} + Al_2O_3 \rightarrow 4\text{YAP}$$

$$3\text{YAP} + Al_2O_3 \rightarrow \text{YAG}$$

In the present case, YAM and YAP are the first phases that develop during the heat treatment, implying that crystallization occurs in the Y-rich regions. With increasing holding time, the phase compositions gradually move to YAP and then YAG, which is associated with an Al-rich phase. The phase evolution indicates that the reaction is carried out by the diffusion of Al^{3+} into Y-rich sites, leading to a phase transformation from YAM to YAP and finally to YAG. SEM patterns shown in Fig. 3 reveal that spherical Y_2O_3 particles retain their original morphology and size during the first minute of heat treatment even though YAM and YAP have already formed. When the holding time is increased to 5 min, spherical particles with sizes of about 400–600 nm clearly emerge (Fig. 3(b)). The particle sizes increase to about 600–900 nm after 30 min, as presented in Fig. 3(c). At this point, YAG becomes the dominant phase in the system. The particles grow to micron-scale proportions when the heat treatment reaches 60 min, as shown in Fig. 3(d), and starts to exhibit vermicular features, which is the typical grain growth characteristic of YAG. Particles observed in the present case all demonstrate moderately uniform size distributions and distinct particle shapes during the entire heating process, up until vermicular growth begins to occur at 60 min holding time.

XRD patterns for [Al_2O_3/Y^{3+}] sample under various heat treatments are shown in Fig. 4. YAG appears after heating for 1 min at 1600 °C, although YAP remains the major phase. The amount of YAG then increases with decreasing YAP 5 min later.

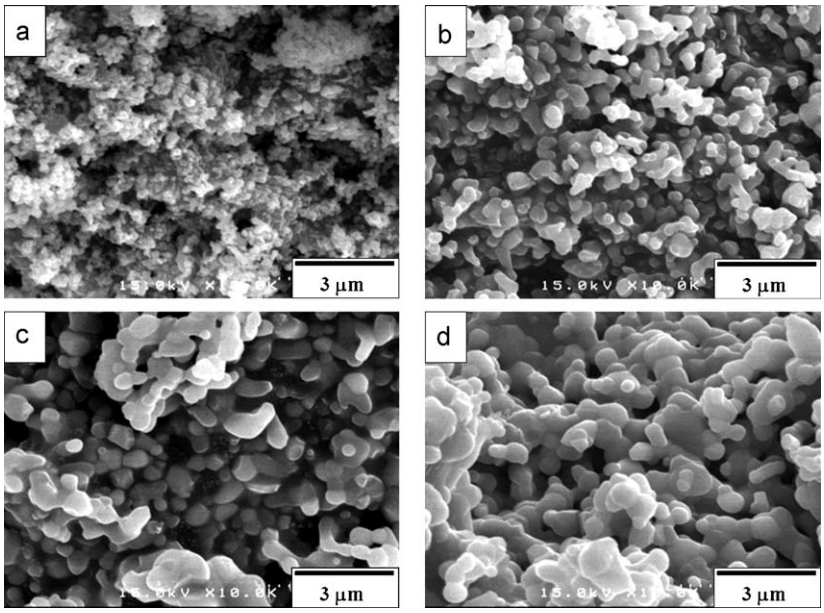

Fig. 3. SEM micrographs of [Y_2O_3/Al^{3+}] annealed at 1600 °C for (a) 1 min, (b) 5 min, (c) 30 min and (d) 60 min.

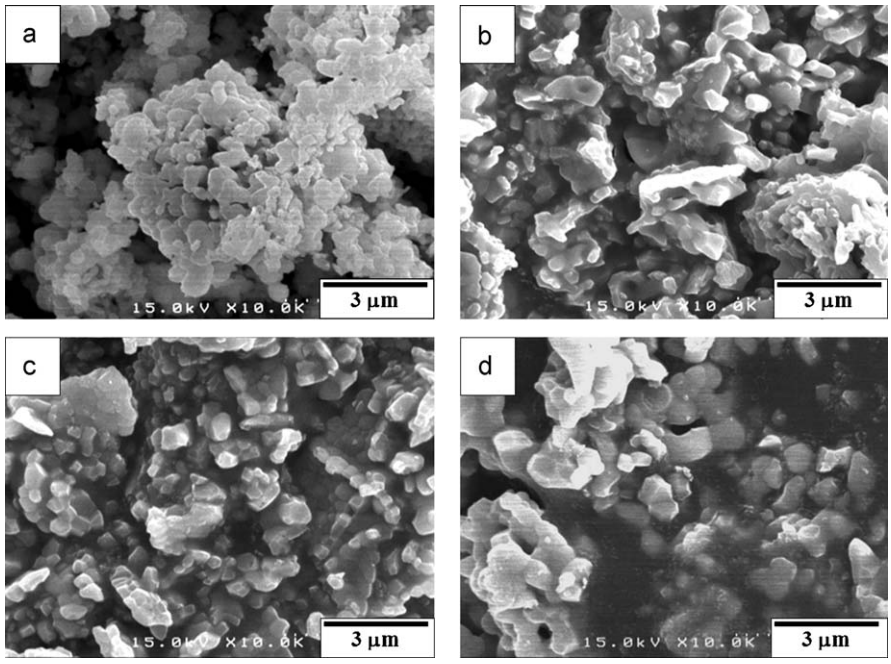

Fig. 5. SEM micrographs of [Al_2O_3/Y^{3+}] annealed at 1600 °C for (a) 1 min, (b) 5 min, (c) 30 min and (d) 60 min.

The reaction appears to cease after 30 min because no apparent variation is observed. Normally, the crystallization temperature of Y_2O_3 is as low as 500 °C[24]; however no Y_2O_3 is ever detected during the entire heating process. In comparison to the [Y_2O_3/Al^{3+}] sample, crystallization seems to take place at Al-rich sites because YAP and YAG are massively generated during the early stages of the heating process and no YAM is formed. The absence of crystallized Y_2O_3 implies that the Y^{3+} ions are rapidly consumed by reacting with α-Al_2O_3, simultaneously giving rise to YAP and YAG. Some YAP particles continue to react with the rest of the α-Al_2O_3 in the system to form YAG with increasing holding time. Other YAP particles, however, remain in the system, probably due to the lack of contact points with the unreacted α-Al_2O_3. One can see from Fig. 5(a) that many small and agglomerated particles are formed after holding for 1 min at 1600 °C; these particles are mainly assigned to the YAP, YAG, and unreacted α-Al_2O_3 crystals. This is supported by the XRD results presented in Fig. 4. The sample is composed of various small crystals with sizes of around 300 nm, as seen in Fig. 5(b). The crystals are relatively aggregated and show slight grain growth with increasing holding time up to 30 min (Fig. 5(c)). More obvious crystal growth is not detected until heating for 60 min, as seen in Fig. 5(d).

According to the experimental results described above, phase transformation is apparently determined by the competition of ionic mobility of the precursor sources. For the [Y_2O_3/Al^{3+}] sample, phase transformation is carried out by the diffusion of Al^{3+} into the Y_2O_3 particles since Y^{3+} is restricted to a crystallized Y_2O_3 crystal that exhibits relatively lower mobility. Therefore, phase transformation follows the sequence YAM to YAP to YAG, corresponding to the evolution of the [Y^{3+}]/[Al^{3+}] ratio from high to low. The as-formed crystals not only retain the distinctive morphology of the starting Y_2O_3 particle but also show rather good dispersion. It is generally accepted that the ionic mobility of Al^{3+} is higher than that of Y^{3+} in the oxide structure.[1] In most Y_2O_3–Al_2O_3 solid-state reactions, the reaction occurs on the Y_2O_3 side and follows the sequence of YAM → YAP → YAG when Al^{3+} migrates gradually into the Y_2O_3 structure. This is generally consistent with the phase transformation behavior displayed by the [Y_2O_3/Al^{3+}] sample. It is also known that the diffusion coefficient of Y^{3+} in polycrystalline Al_2O_3 is in the order of 10^{-6} cm^2 s^{-1}, which is much higher than the self-diffusion of Al^{3+} in Al_2O_3 (smaller than 10^{-12} cm^2 s^{-1}).[25,26] As a consequence, the phase transformation of the [Al_2O_3/Y^{3+}] sample proceeds by the diffusion of Y^{3+} into the Al_2O_3 structure, directly producing Al-rich phases, i.e., YAP and YAG, instead of YAM. The reaction ceases after 30 min of heating, which may be due to the lack of contact points between Al_2O_3 and YAP because of the obstruction created by large crystals of YAG. It has been observed that the chemical diffusion coefficient of Y^{3+}-doped Al_2O_3 shows a sharp decreasing trend between 1560 and 1650 °C due to the precipitation of YAG at the grain boundaries.[27] This is in fair agreement with the present case, where phase transformation is hindered as large YAG crystals are formed. Relatively slight grain growth may also be attributed to the same reason.

3.2. YAH–YAG phase transformation route

The previous section found that phase transformation appears to prefer the YAM–YAP–YAG route where no YAH is ever observed even though one of the precursors is derived from a wet-chemical process. According to a report by Arendt et al.,[28] the mobility of a species in molten salt is in the order of 1×10^{-5} to 1×10^{-8} cm^2 s^{-1}, which is much higher in comparison to its mobility in the solid state (1×10^{-18} cm^2 s^{-1}). The reaction

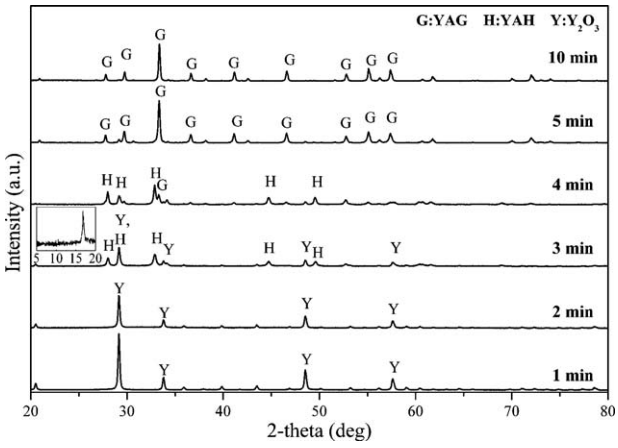

Fig. 6. XRD patterns of [Y_2O_3/Al^{3+}] annealed with NaCl at 1150 °C for 1, 2, 3, 4, 5, and 10 min.

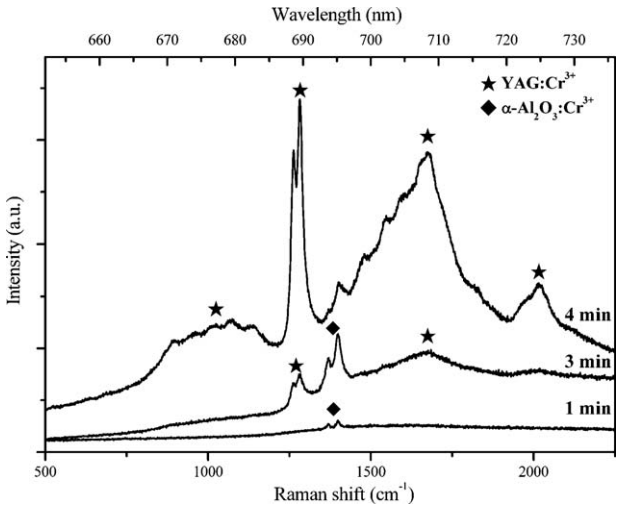

Fig. 7. Raman spectrum of [Y_2O_3/Al^{3+}] sample annealed with NaCl at 1150 °C for 1, 3 and 4 min.

rate can also be significantly accelerated within a short period of time not only because of high ionic mobility but also because of the short diffusion distance in the liquid state.[28] In this section, an NaCl flux is incorporated with the aim of further enhancing ionic mobility. It was found that the reaction rate is effectively accelerated by the flux so that the phase transformation can be completed at a heating temperature as low as 1150 °C within a short span of time. XRD patterns of the [Y_2O_3/Al^{3+}] sample heat treated at 1150 °C for 1–5 min are shown in Fig. 6, showing that the phase transformation was completely altered to the YAH–YAG route by the addition of NaCl flux. XRD patterns shown in Fig. 6 indicate that the peaks corresponding to YAH start to emerge after 3 min, while some unreacted Y_2O_3 still remains. Y_2O_3 is almost completely consumed after 4 min and YAG begins to emerge in the meantime. YAG becomes a single phase after heating at 1150 °C for 5 min. YAM, YAP and α-Al_2O_3 are never found during the phase transformation process from the XRD patterns in this case. Normally Al-rich components should be presented once YAH is produced so that YAG stoichiometry would be maintained; nevertheless, no diffraction peaks associated with the possible Al-related phases are shown even for the sample composed of mainly YAH and a very small amount of Y_2O_3 (1150 °C/3 min). A new hexagonal $Y_3Al_5O_{12}$ structure which exhibits a YAG stoichiometry but similar XRD features to YAH has been proposed.[29] It may explain the absence of Al related phases if the YAH formed here is actually this new hexagonal-YAG structure. However, the peculiar diffraction peaks of hexagonal-YAG related to YAH at around 8.2° (shown in the inset of Fig. 6), 29° and 31° are never found. It implies that the as-formed YAH in the present case is not hexagonal-YAG. Otherwise poor crystallinity or insufficient quantities of these Al-related phases that are out of the detection limit of XRD technique could be the reason why the Al-rich components are invisible in the XRD patterns. For that reason Raman spectroscopy is employed to precisely examine how the excess Al^{3+} ions performed in the system because it provides a better resolution on phase determination than XRD. Fig. 7 shows the Raman spectra of [Y_2O_3/Al^{3+}] sample annealed at 1150 °C for 1, 3, and 4 min, respectively. It is surprisingly found that no apparent Raman bands but intense fluorescent signals corresponding to Cr^{3+} was detected. It is known that Cr^{3+} is commonly coexisted with Al^{3+} and Cr^{3+} doped α-Al_2O_3 (ruby) exhibits a strong red fluorescence even under very low concentration. The presence of Cr^{3+} here probably originates from the impurity in AIP precursor because it was used as received without additional purification. Such fluorescent noise has been also observed in the synthesis of YAG using Al-alkoxide as precursor.[30] The concentration of Cr^{3+} in AIP is negligible according to the elemental characterization of energy-dispersed X-ray spectroscope (EDXS), however its fluorescent behaviors are distinct and provide important information about the phase composition. It is known that Cr^{3+} is nonluminescent in Y_2O_3 or YAH but exhibits a strongly red fluorescence when it is in Al_2O_3 or YAG structure.[3,31] As it demonstrates in Fig. 7 that two characteristic emissions at about 693 nm and 694 nm corresponding to Cr^{3+} ions situated at α-Al_2O_3 are revealed after annealing at 1150 °C for shortly 1 min and becomes quite obvious as the heating duration increases to 3 min. The fluorescence of α-Al_2O_3:Cr^{3+} is weakened after heating for 4 min. In parallel, typical fluorescent spectrum of Cr^{3+} doped YAG containing two sharp R-line emissions at 688 and 689 nm[32] are emerged at 3 min suggesting that a slight amount of YAG has already formed even though it was not detected by XRD. The fluorescence of YAG:Cr^{3+} turns into very intense signals where three phonon sidebands aside the major R-line emission at around 678, 708 and 725 nm[32] are clearly revealed after heating for 4 min. Although Al-rich components were invisible from XRD characterizations, the fluorescent properties of Cr^{3+} clearly manifest that Al ions are gradually crystallized into α-Al_2O_3 phase at the early stage and then react with YAH to form YAG. These results are generally in agreement with the trend observed by XRD analyses but offer more information about the phase composition.

TEM observations for the as-prepared [Y_2O_3/Al^{3+}] sample illustrate that the Y_2O_3 spheres are homogeneously dispersed in the amorphous Al_2O_3 clusters, as shown in Fig. 8(a). The Y_2O_3 spheres completely disappear and some fragmented pieces are

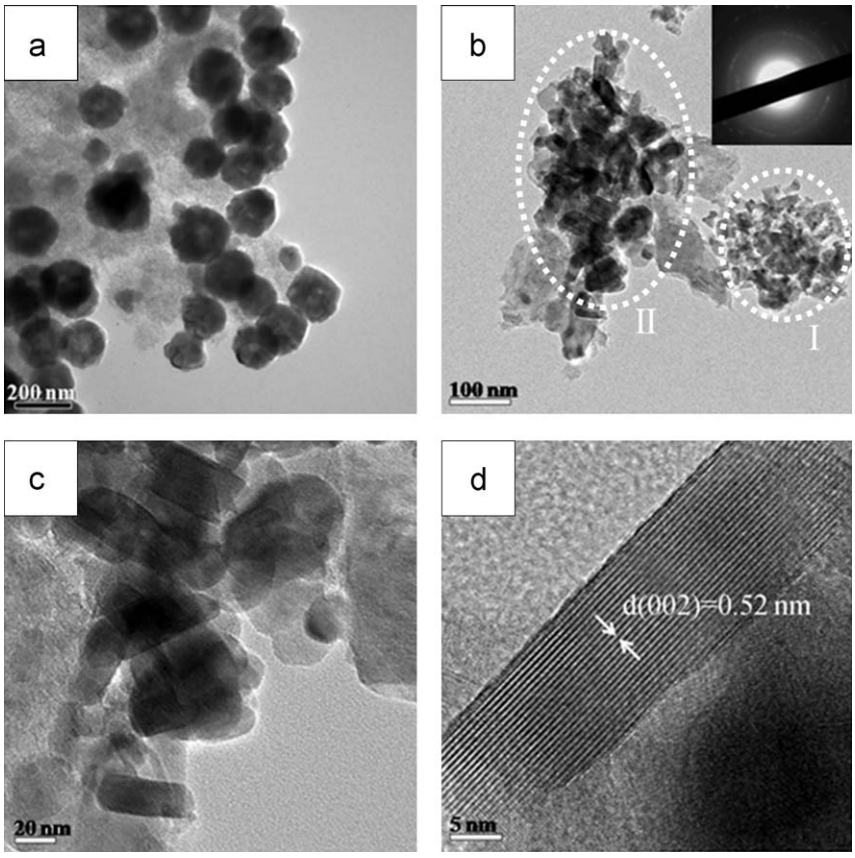

Fig. 8. TEM images [Y_2O_3/Al^{3+}]: (a) as-prepared; (b)–(d) annealed with NaCl at 1150 °C for 3 min.

revealed after heating for 3 min, as shown in the region marked "I" in Fig. 8(b). This fragmented region is composed of both Y and Al according to EDXS analysis and the phase composition is identified as Y_2O_3 polycrystallines and some amorphous matter according to the electron diffraction patterns focused on this fragmented region as illustrated in the inset of Fig. 8(b). This suggests a fact that some of the Al-ions still persist in amorphous state which were not detected by neither XRD nor Raman. The phase transformation via YAH–YAG route is extremely fast, the excess of Al components may not have enough time to all crystallized in α-Al_2O_3 before reacting with YAH to YAG; therefore a partial of them still remain amorphous. An extra experiment was performed in order to verify whether or not Y_2O_3 is dissolved by the molten NaCl flux. In this experiment, Y_2O_3 spheres were individually heated with NaCl at 1150 and 1250 °C for 1 h, respectively. It was found that Y_2O_3 is not soluble in the molten NaCl flux and remains spherical in appearance after heating processes. Apparently, the Y_2O_3 spheres cannot be destroyed by merely the molten NaCl without the existence of Al ions. It is known that if one reactant is more soluble than another in a flux, the former would dissolve into the salt at an earlier stage and induce an in situ reaction to form a product on the surfaces of the reactant that is less soluble.[33] In the present case, Al ions are the ones that dissolved in the molten NaCl so that their mobility (diffusion rate) are greatly increased and as a consequence accelerate the reaction rate. The destruction of Y_2O_3 spheres is evidence showing that an extremely fast reaction is occurred. In parallel, a large amount of rod-like particles are formed at the region marked "II" in Fig. 8(b), a higher magnification of which is shown in Fig. 8(c). These rod-like crystals are consistent with the YAH structure according to the high-resolution TEM image illustrated in Fig. 8(d) and high-resolution electron diffraction patterns. In addition, the as-formed YAH particles are found to exhibit an approximate length of 50 nm and width of 20 nm, obviously smaller than the original size of the Y_2O_3 spheres (200 nm). According to the experimental results described above, the abrupt appearance of YAH (occurring between 2 and 3 min at 1150 °C) implies that its reaction rate is extremely fast. The crystallization of YAH is assumed to proceed via a nucleation and growth mechanism, and the YAH crystal size detected should be the so-called "critical size" during the nucleation process.

On the other hand, the incorporation of the NaCl flux in the [Al_2O_3/Y^{3+}] sample does not exert effects as influential as the previous one. XRD patterns shown in Fig. 9 demonstrate that a few yttrium complex crystals from yttrium nitrate (labeled "*" in the figure) are formed at the first minute; Y_2O_3 starts to crystallize after 2 min. YAM and a small amount of YAP then emerge after 3 and 5 min, respectively. Only a very small amount of YAG is observed after heating for 10 min. In this case the ionic mobility of Y^{3+} seems to be unenhanced by the molten NaCl because Y_2O_3 is crystallized instead of forming YAP or YAG, as was observed at 1600 °C. This was supposed to be due to the low solubility of $Y(NO_3)_3$ in the molten NaCl, such that the

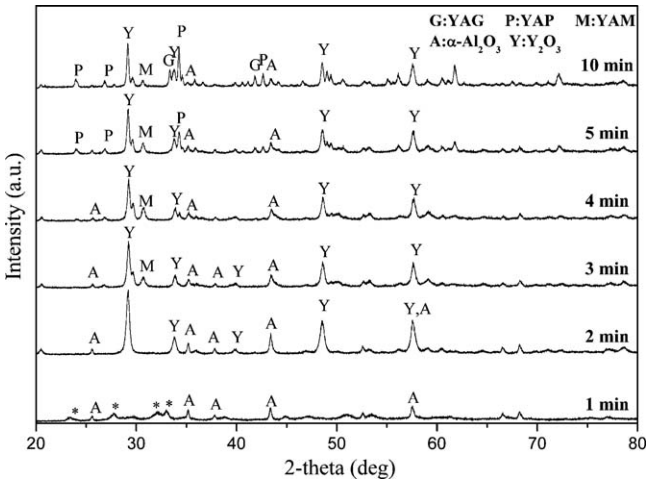

Fig. 9. XRD patterns of $[Al_2O_3/Y^{3+}]$ annealed with NaCl at 1150 °C for 1, 2, 3, 4, 5, and 10 min.

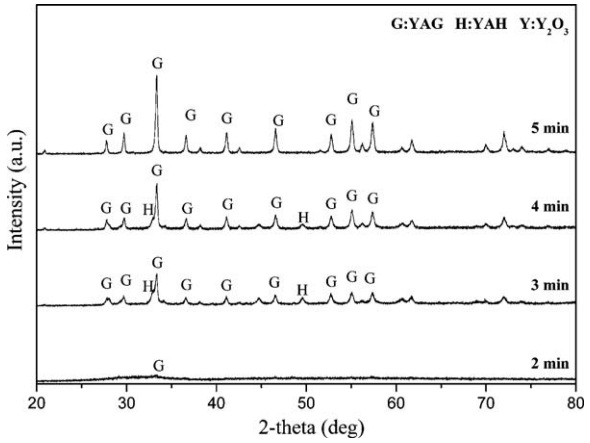

Fig. 10. XRD patterns of the $[Y^{3+}/Al^{3+}]$ annealed with NaCl at 1150 °C for 2, 3, 4, and 5 min.

ionic mobility of Y^{3+} is unsuccessfully promoted. Production of an appropriate flux adapted for $Y(NO_3)_3$ will be attempted in future studies to investigate phase transformation behaviors when the mobility of Y^{3+} ions is effectively promoted.

3.3. Direct YAG crystallization route

The previous results indicate that YAH is generated when the ionic mobility of Al^{3+} is enhanced to induce a nucleation and growth process. The mobility of Al^{3+} is accelerated by means of the addition of a flux. However, Y^{3+} is still confined to a crystallized Y_2O_3 structure, which may somehow restrict the phase transformation rate. In the following work, an analogue of the experiment was performed by replacing the crystallized Y_2O_3 precursor with amorphous Y_2O_3. XRD analyses presented in Fig. 10 show the structural evolution of $[Y^{3+}/Al^{3+}]$ precursor annealed at 1150 °C from 1 to 5 min. It was found that peaks corresponding to the YAG phase appear 2 min after heating and their intensities increase when the heating duration is extended to 3 min. A broad but weak band at the peak of YAG at around 34°, assigned to the YAH phase, is detected when YAG is largely crystallized. This band completely disappears after heating for 5 min. In comparison to the $[Y_2O_3/Al^{3+}]$ sample, the phase transformation in the analogue experiment appears to prefer the direct YAG crystallization route. This result is consistent with many cases observed during wet-chemical synthesis[8–21] and proves that the direct YAG crystallization route cannot be undertaken unless both Y^{3+} and Al^{3+} are highly mobile. In combination with the previous experimental results, the phase transformation route via YAH–YAG is considered to be determined by the local $[Y^{3+}]/[Al^{3+}]$ stoichiometry where the nucleation reaction occurs. In the $[Y_2O_3/Al^{3+}]$ sample, YAH nuclei are formed from the fragmented regions, where some Y_2O_3 nanocrystalline materials remain. This means that the crystallization of YAH actually takes place in relatively Y-rich sites, which is more favorable for the selection of YAH rather than YAG. Once homogeneity (atomic distribution) is improved during the synthetic process, i.e., the $[Y^{3+}/Al^{3+}]$ precursor, YAG becomes predominant and is able to crystallize directly from the system. This result is in agreement with common observations of YAG synthesis via wet-chemical processes, where both Y^{3+} and Al^{3+} are derived from amorphous precursors. This work also confirms that the promotion of YAH is actually developed from the inhomogeneity of stoichiometric distribution, not from the effect of impurities as proposed by Iida et al.,[7] who believed that nitrate compounds more easily induce YAH formation and carbon compounds more readily drive YAG crystallization directly from the amorphous phase. Their findings are in contradiction to that observed in the present work because the $[Y^{3+}/Al^{3+}]$ sample contained nitrate, and yet it followed the direct YAG crystallization route. The $[Y_2O_3/Al^{3+}]$ sample contains carbon compounds, and the YAH–YAG route is selected in this case.

4. Conclusions

It is confirmed that the mobility of Y^{3+} and Al^{3+} ions in the precursors is the key factor that leads phase transformation selection toward different pathways. For ions that exhibit relatively low ionic mobility, for example, those confined to a crystallized structure, phase transformation prefers the conventional YAM–YAP–YAG route. The competition of ionic mobilities between Y^{3+} and Al^{3+} determines the selection of the transition phase during phase transformation: the Y-rich phase (YAM) is selected when the mobility of Al^{3+} is higher than that of Y^{3+}, whereas YAP or YAG is formed when the mobility of Y^{3+} is higher than that of Al^{3+}. YAH occurs only when the mobility of Al^{3+} is effectively enhanced by a molten NaCl salt flux; in this case, a rapid nucleation and growth reaction is induced. It is observed that YAH exhibits a rod-like morphology and shows a critical size of about 20 nm × 50 nm during the nucleation process. Inhomogeneity is determined to be the major factor that generates YAH when the reaction is nucleation and growth-dominated; otherwise YAG is directly and rapidly crystallized from amorphous precursors without passing through any intermediate phases.

References

1. Neiman AY, Tkachenko EV, Kvichko LA, Kotok LA. Conditions and macromechanism of the solid-phase synthesis of yttrium aluminates. *Russ J Inorg Chem* 1980;**25**:1294–7.
2. Glushkova VB, Krzhizhanovskaya VA, Egorova ON, Udalov YP, Kachalova LP. Interaction of yttrium and aluminum oxide. *Inorg Mater* 1983;**19**:95–9.
3. Kinsman KM, McKittrick J. Phase development and luminescence in chromium-doped yttrium aluminum garnet (YAG: Cr) phosphors. *J Am Soc* 1994;**77**:2866–72.
4. Johnson BR, Kriven WM. Crystallization kinetics of yttrium aluminum garnet ($Y_3Al_5O_{12}$). *J Mater Res* 2001;**16**:1795–805.
5. Marsubara I, Paranthaman M, Allison SW, Cates MR, Beshears DL, Holcomb DE. Preparation of Cr-doped $Y_3Al_5O_{12}$ phosphors by heterogeneous precipitation methods and their luminescent properties. *Mater Res Bull* 2000;**35**:217–24.
6. Adylov GT, Voronov GV, Mansurova EP, Sigalov LM, Urazveva EM. Y_2O_3–Al_2O_3 system higher 1473 K. *Russ J Inorg Chem* 1988;**33**:1867–9.
7. Iida Y, Towata A, Tsugoshi T, Furukawa M. In situ Raman monitoring of low temperature synthesis of YAG from different starting materials. *Vibra Spectro* 1999;**19**:399–405.
8. Yamaguchi O, Matui K, Shimizu K. Formation of $YAlO_3$ with garnet structure. *Ceram Int* 1985;**11**:107–8.
9. Veitch CD. Synthesis of polycrystalline yttrium iron garnet and yttrium aluminum garnet from organic precursors. *J Mater Sci* 1991;**26**:6527–32.
10. Hess NJ, Maupin GD, Chick LA, Sunberg DS, McCreedy DE, Armstrong TR. Synthesis and crystallization of yttrium–aluminium garnet and related compounds. *J Mater Sci* 1994;**29**:1873–8.
11. MacKenzie KJD, Kemmitt T. Evolution of crystalline aluminates from hybrid gel-derived precursors studied by XRD and multinuclear solid-state MAS NMR. II. Yttrium-aluminium garnet, $Y_3Al_5O_{12}$. *Thermochim Acta* 1999;**325**:13–8.
12. Nyman M, Caruso J, Hampden-Smith MJ. Comparison of solid-state and spray-pyrolysis synthesis of yttrium aluminate powders. *J Am Ceram Soc* 1997;**80**:1231–8.
13. Ullal CK, Balasubramaniam KR, Gandhi AS, Jayaram V. Non-equilibrium phase synthesis in Al_2O_3–Y_2O_3 by spray pyrolysis of nitrate precursors. *Acta Mater* 2001;**49**:2691–9.
14. Mah TI, Parthasarathy TA, Kerans RJ. Processing, microstructure, and strength of alumina-YAG eutectic polycrystals. *J Am Ceram Soc* 2000;**83**:2088–90.
15. Gowda G. Synthesis of yttrium aluminates by the sol–gel process. *J Mater Sci Lett* 1986;**5**:1029–32.
16. Tachiwaki T, Yoshinaka M, Hirota K, Ikegami T, Yamaguchi O. Novel synthesis of $Y_3Al_5O_{12}$ (YAG) leading to transparent ceramics. *Solid State Commun* 2001;**119**:603–6.
17. Cinibulk MK. Synthesis of yttrium aluminum garnet from a mixed-metal citrate precursor. *J Am Ceram Soc* 2000;**83**:1276–8.
18. Apte P, Burke H, Pickup H. Synthesis of yttrium aluminum garnet by reverse strike precipitation. *J Mater Res* 1992;**7**:706–11.
19. Kakade MB, Ramanathan S, Ravindran PV. Yttrium aluminum garnet powders by nitrate decomposition and nitrate-urea solution combustion reactions—a comparative study. *J Alloys Compd* 2003;**350**:123–9.
20. Wang H, Gao L, Niihara K. Synthesis of nanoscaled yttrium aluminum garnet powder by the co-precipitation method. *Mater Sci Eng* 2000;**A288**:1–4.
21. Messier DR, Gazza GE. Synthesis of $MgAl_2O_4$ and $Y_3Al_5O_{12}$ by thermal decomposition of hydrated nitrate mixtures. *Am Ceram Soc Bull* 1972;**51**:692–7.
22. Gandhi AS, Levi CG. Phase selection in precursor-derived yttrium aluminum garnet and related Al_2O_3–Y_2O_3 compositions. *J Mater Res* 2005;**20**:1017–25.
23. Li JG, Li X, Sun X, Ikegami T, Ishigaki T. Uniform colloidal spheres for $(Y_{1-x}Gd_x)_2O_3$ ($x = 0$–1): formation mechanism, compositional impacts, and physico chemical properties of the oxides. *Chem Mater* 2008;**20**:2274–81.
24. Hussein GAM. Formation of high surface-area yttrium oxide by the thermal decomposition of different inorganic precursors. *Thermochim Acta* 1994;**244**:139–51.
25. Moya EG, Moya F, Lesage B, Loudjani MK, Grattepain C. Yttrium diffusion in α-alumina single crystal. *J Euro Ceram Soc* 1998;**18**:591–4.
26. Paladio AE, Kingery WD. Aluminum ion diffusion in aluminum oxide. *J Chem Phys* 1962;**37**:957–62.
27. Lesage B, Huntz AM, Petot-ervas G. Transport phenomena in undoped and chromium or yttrium doped-alumina. *Radiat Eff Defects Solids* 1983;**75**:283–99.
28. Arendt RH, Rosolowski JH, Szymaszek JW. Lead zirconate titanate ceramics from molten salt solvent synthesized powders. *Mater Res Bull* 1979;**14**:703–9.
29. Laine RM, Marchal J, Sun H, Pan XQ. A new $Y_3Al_5O_{12}$ phase produced by liquid-feed flame spray pyrolysis (LF-FSP). *Adv Mater* 2005;**17**:830–3.
30. Wu YC. *Planar waveguides of Y_2O_3, Y_2O_3: Tb^{3+} and $Y_3Al_5O_{12}$ (YAG) elaborated by sol–gel process: structural and optical analyses*, Ph.D. thesis. University of Claude Bernard Lyon 1; 2005.
31. Pillonnet A, Garapon C, Champeaux C, Bovier C, Jaffrezic H, Mugnier J. Fluorescence of Cr^{3+} doped alumina optical waveguides prepared by pulsed laser deposition and sol–gel method. *J Lumin* 2000;**87–89**:1087–9.
32. Shen YR, Bray KL. Effect of pressure and temperature on the lifetime of Cr^{3+} in yttrium aluminum garnet. *Phys Rev B* 1997;**56**:10882–97.
33. Byrappa K, Ohachi T. *Crystal growth technology*. New York: Springer; 2002.